ISSN: 2710-0588

Research on Air-Ground Time-Frequency Synchronization Based on Microwave Two-Way Pseudorange Measurement

Jiaming Xiong[1], Daopeng Dong[1,*], Jun Xu[1], Haoxin Zhao[1]

[1]Chengdu Spaceon Electronics Co., Ltd., Chengdu 610036, China

[*] Corresponding author. E-mail: 2535244@qq.com

Abstract

To meet the requirements of distributed air-ground nodes for a unified time reference, state-data exchange, and low power consumption, this paper presents an integrated time-frequency synchronization and microwave communication system based on dual one-way ranging (DOWR). The proposed scheme adopts frequency-duplex C-band links and spread-spectrum BPSK signaling. Gold-code CDMA is employed on the uplink to support access by multiple slave nodes. The information rate is 1 kbit/s and becomes 2 kbit/s after LDPC coding. A truncated Gold code with a chip rate of 10.23 Mchip/s and a length of 10,230 chips is used for ranging, time-frequency comparison, and data transmission. Models for range and clock-offset estimation are derived, and equipment-delay calibration, link-budget analysis, and the system workflow are presented. For design distances of 25, 50, and 120 km, the calculated link margins remain sufficient, while the engineering communication boundary is set to 255 km. The cross-correlation peak of the selected spreading codes is more than 14 dB below the autocorrelation peak. The proposed architecture enables relative timing synchronization, 10 MHz frequency disciplining, and low-rate data return over a common microwave link.

Keywords

Dual one-way ranging; time-frequency synchronization; spread-spectrum communication; Gold codes; link budget; air-ground integration.

1. Introduction

Integrated air-ground measurement and control, communication-navigation fusion, and low-orbit aerospace missions generally require multiple spatial nodes and ground nodes to share a unified time reference. In scenarios where nodes are geographically dispersed, fiber links cannot be deployed, or GNSS signals are obstructed or interfered with, one-way timing alone cannot adequately suppress propagation delay, equipment delay, and clock drift. Moreover, separate implementation of time-frequency synchronization and communication links increases spectrum occupancy, power consumption, and equipment weight. Therefore, completing high-precision time-frequency comparison and low-rate state-data return over the same microwave link is an effective way to improve system integration and engineering adaptability.

Two-way satellite time and frequency transfer (TWSTFT) cancels most common propagation errors by exploiting the symmetry of the uplink and downlink, and has become an important means of remote clock comparison [1]. Recent microwave two-way time-synchronization methods for low-orbit payloads and ground stations have further accounted for orbit, attitude, and phase-center calibration errors, demonstrating the feasibility of high-precision air-ground time synchronization over microwave links [2]. Unlike transponder-based satellite TWSTFT, the dual one-way pseudorange measurement investigated in this paper establishes direct forward and reverse links between a master node and a slave node. It features a simple link

ISSN: 2710-0588

structure, simultaneous range and clock-offset outputs, and convenient networking with ground equipment.

In terms of communication architecture, direct-sequence spread spectrum provides anti-jamming capability, low probability of intercept, and code-division multiple access. Gold codes offer a favorable tradeoff among autocorrelation, cross-correlation, and family size, and have been widely used in CDMA spreading-sequence design [3-6]. LDPC codes provide near-capacity error-correction performance and a decoding structure suitable for parallel implementation, making them an important coding scheme in modern high-reliability communication systems [7-8]. Accordingly, this paper combines spread-spectrum ranging, CDMA multiple access, LDPC channel coding, and a clock-disciplining loop to form an integrated timing and communication air-ground microwave link.

The main contributions of this paper are as follows. First, the temporal measurement model of dual one-way ranging is established, and formulas for range and clock-offset estimation are derived, together with an analysis of equipment delay and path non-reciprocity. Second, an integrated communication architecture is designed with C-band frequency division, spread-spectrum BPSK, uplink Gold-code CDMA, and LDPC coding. Third, under explicit engineering assumptions, link-budget verification and correlation analysis of the truncated Gold code are performed. Finally, a complete system workflow is presented, covering startup and link acquisition, time-frequency disciplining, and holdover after link interruption. The results provide a basis for system design, equipment development, and field-test parameter determination.

2. Principle of Dual One-Way Ranging

2.1. Measurement Model and Variable Definitions

Let the master node be the time reference and the slave node be the disciplined node. Both nodes transmit forward and reverse ranging signals under the control of their local clocks, and frame-synchronization delays are obtained from pseudocode-phase and carrier-phase measurements. Because the two directions are measured almost simultaneously, the common propagation delay is retained in the sum term, whereas the clock offset between the two nodes is separated in the difference term. Figure 1 shows the timing relationship of dual one-way ranging.

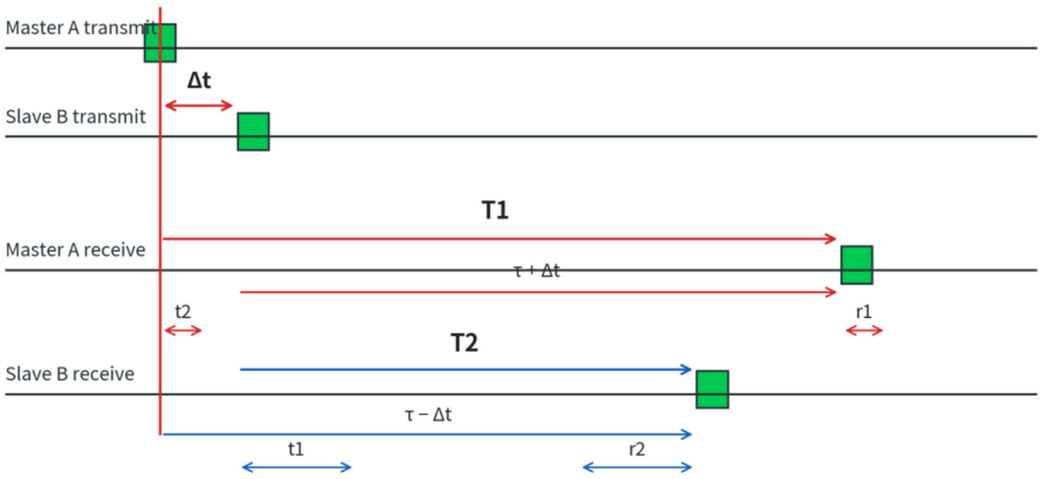


Figure 1. Timing relationship of dual one-way ranging

ISSN: 2710-0588

Table 1. Variable definitions for the two-way measurement model

Symbol	Unit	Definition
T_1, T_2	s	Frame-synchronization delay measurements obtained by the master and slave nodes
t_1, t_2	s	Transmit-channel equipment delays of the master and slave nodes
r_1, r_2	s	Receive-channel equipment delays of the master and slave nodes
t_{12}, t_{21}	s	Equivalent equipment-delay sums in the master-to-slave and slave-to-master directions
τ	s	Approximately reciprocal spatial propagation delay in the two directions
Δt	s	Clock offset of the slave relative to the master, i.e., slave clock reading minus master clock reading
D, c	m, m/s	True distance between the master and slave nodes and the speed of light in vacuum

2.2. Range and Clock-Offset Estimation

According to the timing relationship in Fig. 1, the reverse frame-synchronization delay measured by the master contains the slave transmit delay, propagation delay, master receive delay, and clock offset. Similarly, the forward frame-synchronization delay measured by the slave contains the master transmit delay, propagation delay, slave receive delay, and the negative clock offset. The two measurements can be written as

$$T_1 = t_2 + \tau + r_1 + \Delta t \tag{1}$$

$$T_2 = t_1 + \tau + r_2 - \Delta t \tag{2}$$

The equivalent equipment delays in the two directions are defined as

$$t_{12} = t_1 + r_2 \tag{3}$$

$$t_{21} = t_2 + r_1 \tag{4}$$

Assuming approximately reciprocal propagation paths and calibrated equipment delays, the distance and clock offset can be obtained from Eqs. (1)–(4):

$$D = c/2 \cdot [(T_1 + T_2) - (t_{12} + t_{21})] \tag{5}$$

$$\Delta t = 1/2 \cdot [(T_1 - T_2) + (t_{12} - t_{21})] \tag{6}$$

ISSN: 2710-0588

Equation (5) shows that the sum of the two one-way measurements eliminates the first-order clock offset and yields the range, while Eq. (6) shows that the difference separates the clock offset. In engineering practice, T_1 and T_2 are calculated from local delay measurements extracted by the code tracking loops. Equipment delays are obtained through closed-loop calibration, standard delay lines, or field comparison. Clock offsets from successive epochs can be used to estimate clock drift and drive the slave frequency-standard disciplining loop so that the 1PPS phase and 10 MHz frequency are progressively locked to the master reference.

2.3. Error Sources and Calibration

If the forward and reverse propagation delays are not fully reciprocal, let their deviations from the nominal propagation delay τ be $\delta\tau_1$ and $\delta\tau_2$, respectively. Common-mode and differential errors are then introduced into the range and clock-offset estimates:

$$\hat{D} = D + c/2 \cdot (\delta\tau_1 + \delta\tau_2) \tag{7}$$

$$\Delta\hat{t} = \Delta t + 1/2 \cdot (\delta\tau_1 - \delta\tau_2) \tag{8}$$

Therefore, the link design should ensure stable antenna phase centers in both directions and consistent temperature characteristics of the transmit and receive channels. Ionospheric, tropospheric, multipath, and equipment group-delay terms should also be calibrated. For short-baseline air-ground links, path non-reciprocity is generally smaller than that of long-baseline satellite links. Nevertheless, when the low-altitude link elevation changes rapidly or ground multipath is significant, two-way carrier-phase smoothing, epoch filtering, and link-availability criteria are still required to suppress outliers. Long-term equipment-delay drift should be incorporated into periodic calibration procedures.

3. Integrated Air-Ground Microwave Communication System Design

3.1. Frequency Selection

The bidirectional link operates in the C band with transmit and receive frequency separation for the following reasons. First, although higher frequency bands provide wider available bandwidth, their narrower antenna beams are unfavorable for one-to-many node access and link maintenance under attitude disturbance. Second, power-amplifier efficiency decreases as the operating frequency increases, so a lower frequency helps reduce power consumption and thermal-design pressure. Third, for the same link conditions, C-band rain attenuation and atmospheric absorption are smaller than those at higher frequency bands. Fourth, free-space path loss is proportional to the square of frequency, so a lower frequency helps extend communication coverage. Considering device maturity, power consumption of airborne equipment, and networking requirements, the uplink transmit frequency F_1 is selected as 7.4 GHz±50 MHz, and the downlink transmit frequency F_2 is 6.9 GHz±50 MHz. These frequencies are customized transmit/receive assignments for the system and should be coordinated with mission frequency resources and radio-management requirements before deployment.

3.2. Signal Architecture

The bidirectional link between the master and slave nodes adopts an integrated timing and communication design. Ranging pseudocodes, time-frequency comparison data, and node-status data share the same physical link and use direct-sequence spread spectrum with BPSK modulation. The downlink is mainly a broadcast or point-to-point link from the master to the slaves, while different Gold spreading codes distinguish multiple slave nodes on the uplink. The information rate is 1 kbit/s. After LDPC coding with an approximate code rate of 1/2, the

ISSN: 2710-0588

transmitted rate is 2 kbit/s. LDPC decoding with interleaving improves the reliability of low-rate status data under fading and burst-interference conditions. The signal design is summarized in Table 2.

Table 2. Signal-system design

Link	Modulation	Multiple access	Information rate	Channel coding
Master to slave (downlink)	Spread spectrum + BPSK	Broadcast/point-to-point	1 kbit/s	LDPC; 2 kbit/s after coding
Slave to master (uplink)	Spread spectrum + BPSK	Gold-code CDMA	1 kbit/s	LDPC; 2 kbit/s after coding

3.3. Frame Structure and Communication Protocol

The data-frame period is 1 s and mainly carries a two-way comparison service segment and an internal status-data segment. The frame header supports rapid acquisition and frame synchronization. The service segment contains the second count, pseudorange, clock drift, carrier-to-noise density ratio, and node-validity flags. The data segment reserves fields for node expansion and system status information, while a CRC check is placed at the end of the frame. The frame structure is shown in Fig. 2, and the core protocol fields are listed in Table 3.

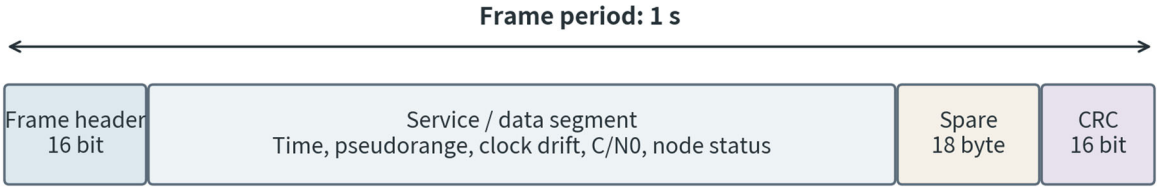


Figure 2. Integrated data-frame structure

Table 3. Core fields of the bidirectional microwave communication protocol

Byte index	Length	Field definition	Remarks
0–1	2	Frame header (FEC8)	Frame synchronization
2–5	4	Time	Unit: s
6–15	10	Node 1: pseudorange, clock drift, C/N_0, measurement-valid flag	Pseudorange unit: 0.1 ns; clock-drift unit: 0.1 Hz
16–95	80	Data for nodes 2–9	10 bytes per node; same structure as node 1
96–105	10	Data for node 10	Supports master-slave network expansion
106–123	18	Spare	Reserved for expansion
124–125	2	CRC check	Frame-integrity check

ISSN: 2710-0588

Note: When a slave node reports only one measurement set, its pseudorange, clock drift, C/N_0, and valid flag may be placed in the node-1 fields, with the remaining node fields set to reserved values.

4. Link Budget and Operating-Range Verification

4.1. Design Case and Assumptions

The original design requirement specifies that the link should support a 1 kbit/s information rate at operating distances of 25, 50, and 120 km with adequate margin. After considering equipment implementation, propagation fading, and networking interference, the maximum engineering operating distance is set to 255 km. To make the budgeting method transparent and reproducible, this section presents an explicit design case. The transmit power, antenna gains, losses, and receiver noise figure are engineering assumptions for the conceptual-design stage and do not represent measured equipment specifications.

Table 4. Assumptions for the link-budget design case

Parameter	Design value	Remarks
Transmit power P_t	30 dBm (1 W)	Engineering assumption; adjustable according to device capability
Transmit/receive antenna gains G_t, G_r	5 dBi / 5 dBi	Engineering assumption including antenna-pattern constraints
Transmit/receive channel losses L_t, L_r	2 dB / 2 dB	Sum of cable, connector, and pointing losses
Atmospheric and rain margin L_a	3 dB	Conservative value for conceptual design
Receiver noise figure NF	3 dB	Engineering assumption
Information rate R_b	2 kbit/s	Rate after LDPC coding
Pseudocode rate R_c	10.23 Mchip/s	Determined by the spreading-code design
Required E_b/N_0	4 dB	Engineering threshold for BPSK with LDPC
System implementation margin M_sys	10 dB	Covers implementation loss, interference, and fading uncertainty

4.2. Budget Model

The free-space path loss is

$$L_{fs} = 92.45 + 20\lg(f_{GHz}) + 20\lg(d_{km}) \quad (dB) \tag{9}$$

The received power, carrier-to-noise-density ratio, spread-spectrum processing gain, and link margin are

ISSN: 2710-0588

$$P_r = P_t + G_t - L_t - L_fs + G_r - L_r - L_a \quad (10)$$

$$C/N_0 = P_r + 174 - NF \quad (11)$$

$$G_p = 10\lg(R_c/R_b) \quad (12)$$

$$M = C/N_0 - [(E_b/N_0)_req + 10\lg(R_b) - G_p] - M_sys \quad (13)$$

Here, P_r is in dBm, C/N_0 is in dB·Hz, G_p is the spread-spectrum processing gain, and M is the link margin after the system implementation margin. For the parameters in Table 4, G_p = 37.09 dB and the required equivalent C/N_0 is approximately −0.08 dB·Hz.

Table 5. Link-budget results for typical operating distances (design case)

Parameter	25 km uplink	25 km downlink	120 km uplink	255 km uplink	255 km downlink
L_fs, dB	137.79	137.19	151.42	157.97	157.36
P_r, dBm	−104.79	−104.19	−118.42	−124.97	−124.36
C/N_0, dB·Hz	66.21	66.81	52.58	46.03	46.64
Link margin M, dB	56.28	56.89	42.66	36.11	36.72

Note: At 50 km, the uplink and downlink margins are 50.26 dB and 50.87 dB, respectively, satisfying the design requirement for 25–120 km.

The budget results show that the margin at 255 km remains approximately 36 dB. This indicates that 255 km is not the thermal-noise theoretical limit. Rather, it is a conservative engineering boundary determined by comprehensively considering equipment-implementation margin, propagation uncertainty, co-site interference, availability requirements, and mission risk. During equipment development, the assumptions in Table 4 should be replaced with measured equivalent isotropic radiated power, receiver G/T, channel group delay, and bit-error-rate curves, and the budget should be closed again.

5. CDMA Spreading-Code Design

5.1. Code Parameters and Generator Polynomials

CDMA is used when multiple slave nodes access the master node. Different pseudocodes distinguish users within the same frequency assignment, saving frequency resources and facilitating system expansion. The design uses an N=14 preferred pair of m-sequences to construct Gold codes, followed by truncation and selection to obtain engineering code words. The pseudocode rate is 10.23 Mchip/s, the code length is 10,230 chips, and the code period is 1 ms. The generator polynomials are

$$G_1(x) = x^{14} + x^{12} + x^{11} + x + 1 \quad (14)$$

$$G_2(x) = x^{14} + x^{12} + x^{11} + x^{10} + x^9 + x^7 + x^4 + x^3 + 1 \quad (15)$$

ISSN: 2710-0588

A classical Gold-code family is formed by two preferred m-sequences and their phase combinations, offering a large family size and low three-valued cross-correlation peaks [3-6]. This design does not use the unscreened full family. Instead, under the truncation constraint of 10,230 chips, 91 engineering code words are selected according to balance, autocorrelation sidelobe, and cross-correlation peak criteria, thereby reducing multiple-access interference and simplifying hardware implementation.

5.2. Correlation Characteristics

Figures 3 and 4 show the normalized autocorrelation curve of the first pseudocode and its normalized cross-correlation curves with the other pseudocodes. The sharp autocorrelation main peak facilitates code-phase acquisition and precise delay measurement, while the generally low cross-correlation peaks suppress inter-code interference when multiple nodes access the network simultaneously. According to the statistical results provided in the source material, the maximum cross-correlation peak between code groups is more than 14 dB below the autocorrelation peak, satisfying the design requirement of a one-to-many networked link.

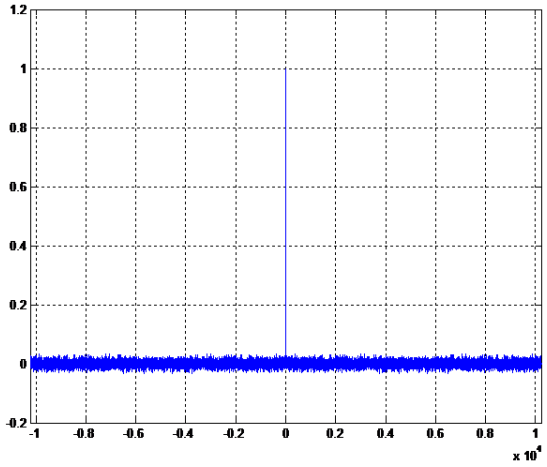


Figure 3. Autocorrelation curve of the first spreading code

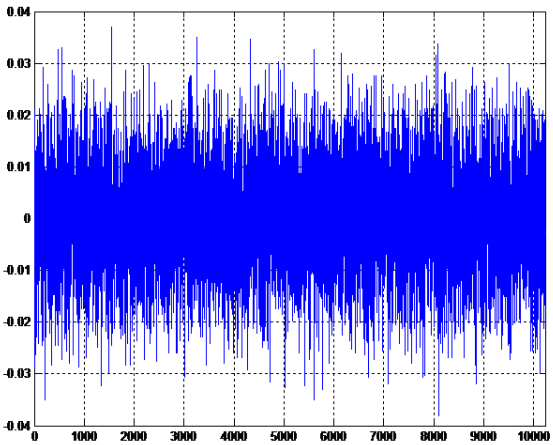


Figure 4. Cross-correlation curves between the first spreading code and the other codes

At the receiver, parallel correlation and threshold detection can be used in the acquisition stage to shorten the search time, while a delay-locked loop maintains code-phase tracking. For

ISSN: 2710-0588

dynamic air-ground links, code-Doppler compensation should be combined with carrier-Doppler estimation to prevent correlation-peak drift over a long code period.

6. System Workflow

After power-on, the timing unit first preheats the rubidium frequency standard and verifies lock. The master can be traceable to GNSS or an external standard time source. After preheating, the slave enters a local holdover state and periodically attempts to establish a bidirectional microwave link with the master. Once the link is established, the two nodes perform dual one-way ranging according to the model in Section 1 and exchange pseudorange, clock drift, C/N_0, and measurement-validity flags in the frame service segment. The slave then adjusts its local frequency standard in real time according to the estimated clock offset and drift, achieving relative synchronization of the 1PPS phase and 10 MHz frequency. The system workflow is shown in Fig. 5.

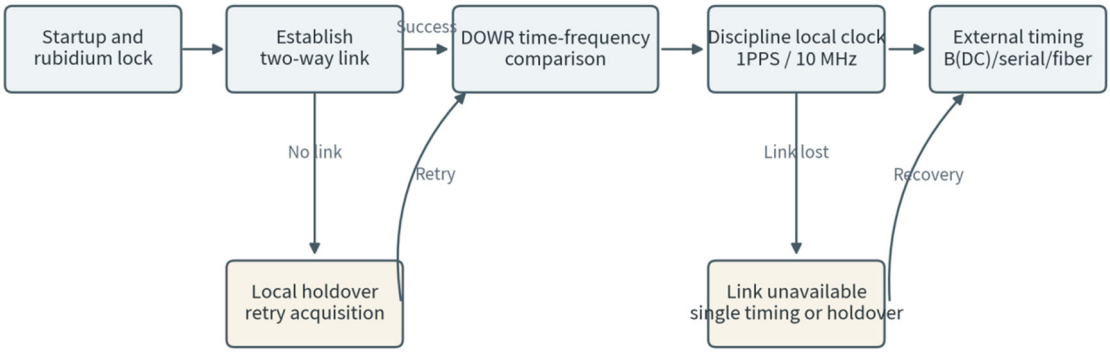


Figure 5. System workflow

When the bidirectional link is interrupted by occlusion, attitude variation, or interference, the system first switches to local single-point timing mode and uses its frequency-holdover capability to maintain the output. If single-point timing is also unavailable, the system enters holdover mode and continues attempting link recovery. After the link is restored, measurement convergence and clock disciplining are re-established to avoid phase jumps in user equipment. The master and slave can also output timing information through 1PPS, B(DC)-code, serial-port, and other interfaces. Ground-station equipment can further extend one-master-multiple-slave high-precision time comparison through a fiber-optic comparison interface.

7. Experimental Verification

Multiple flight tests with airborne microwave comparison systems were carried out on an unmanned-aerial-vehicle (UAV) platform. The tests demonstrated that the comparison performance is negligibly affected by the dynamic environment and shows no significant degradation; however, it is strongly affected by multipath. The verification results are as follows.

7.1. Two-Platform Hover at 100 m Altitude and 400 m Separation

Synchronization performance: standard deviation 0.975 ns, peak-to-peak value 5.1 ns.

ISSN: 2710-0588

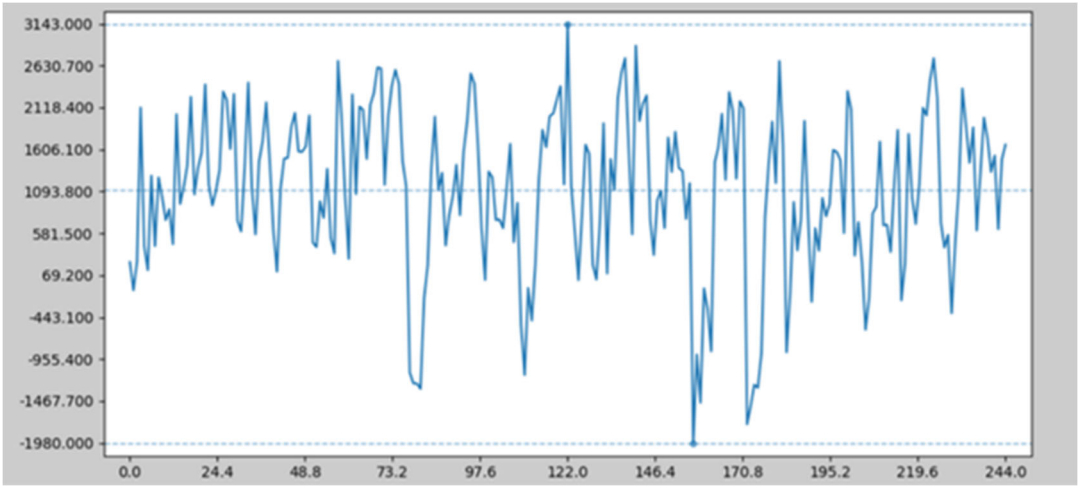


Figure 6. Inter-station time offset of the slave node

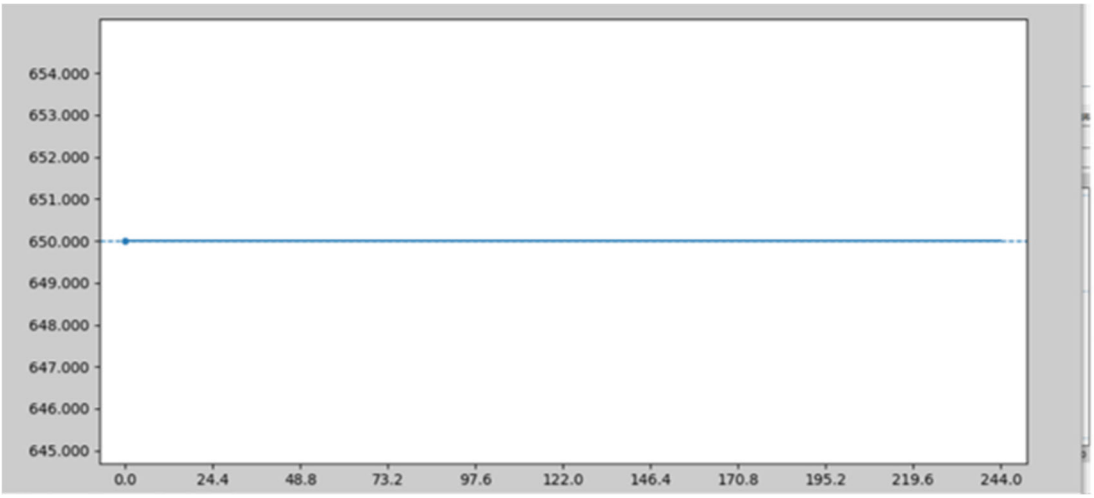


Figure 7. C/N_0 of the slave node (3.3 GHz link)

7.2. Two-Platform Hover at 200 m Altitude and 300 m Separation

Synchronization performance: standard deviation 0.690 ns, peak-to-peak value 3.86 ns.

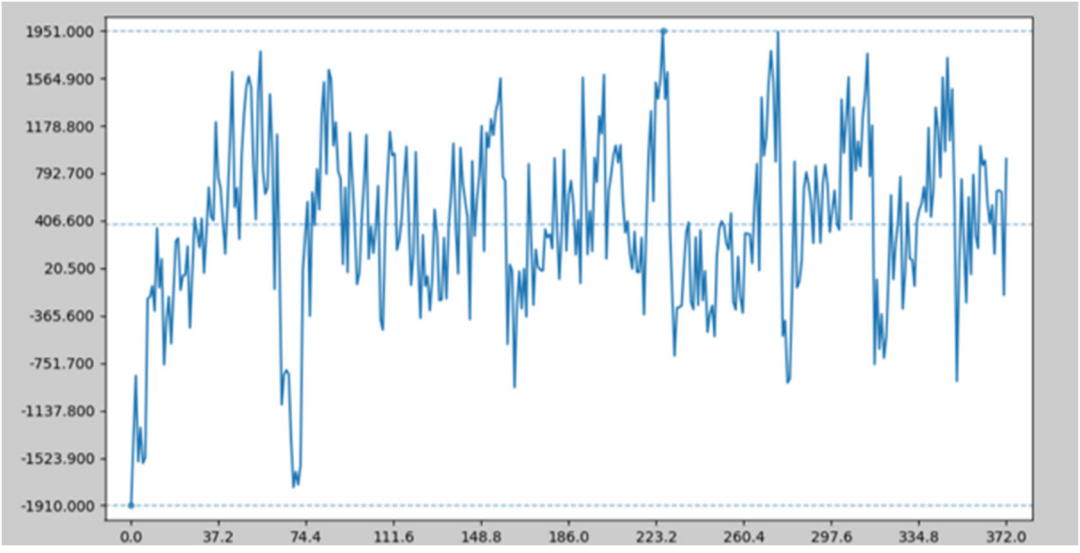


Figure 8. Inter-station time offset of the slave node

ISSN: 2710-0588

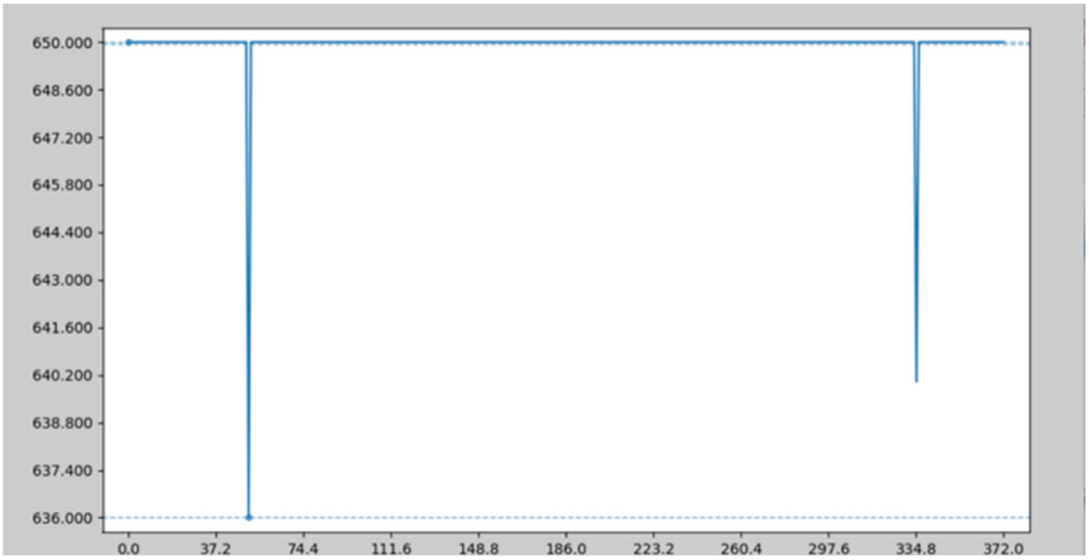


Figure 9. C/N_0 of the slave node (3.5 GHz link)

8. Conclusion

This paper has presented an integrated time-frequency synchronization and microwave communication system for air-ground distributed nodes based on dual one-way pseudorange measurement. The main conclusions are as follows.

(1) The proposed two-way measurement model can simultaneously estimate the inter-node distance and clock offset from two one-way pseudoranges. Under approximately reciprocal paths and calibrated equipment delays, summation and differencing of the two measurements suppress the common clock term and common propagation term, respectively, providing a measurement basis for 1PPS phase synchronization and 10 MHz frequency disciplining.

(2) The system integrates C-band frequency division, spread-spectrum BPSK, uplink Gold-code CDMA, and LDPC coding, using a 1 s frame period to carry time-frequency comparison and node-status data. The design case shows adequate link margins at 25, 50, and 120 km. The 255 km boundary is a conservative engineering limit after comprehensive risk assessment; actual performance should be confirmed through measured budgets and field tests.

(3) The designed 10.23 Mchip/s, 10,230-chip truncated Gold code supports both ranging and multiple access. The cross-correlation peaks of the selected code words are more than 14 dB below the autocorrelation peak, enabling networking of multiple slave nodes. Future work will focus on long-term equipment-delay calibration, loop optimization under dynamic multipath conditions, and field verification of synchronization accuracy.

References

[1] Wu, W. J., Dong, S. W., Li, H. X., et al. (2014). Two-way satellite time and frequency transfer: Overview, recent developments and application. In Proceedings of 2014 European Frequency and Time Forum (EFTF) (pp. 121–125). https://doi.org/10.1109/EFTF.2014.7331442.

[2] Guo, Y., Gao, S., Bai, Y., et al. (2022). A new space-to-ground microwave-based two-way time synchronization method for next-generation space atomic clocks. Remote Sensing, 14(3), 528. https://doi.org/10.3390/rs14030528

[3] Gold, R. (1968). Maximal recursive sequences with 3-valued recursive cross-correlation functions. IEEE Transactions on Information Theory, 14(1), 154–156.

[4] Sarwate, D. V., & Pursley, M. B. (1980). Crosscorrelation properties of pseudorandom and related sequences. Proceedings of the IEEE, 68(5), 593–619.

ISSN: 2710-0588

[5] Turkmani, A. M. D., & Goni, U. S. (1993). Performance evaluation of maximal-length, Gold and Kasami codes as spreading sequences in CDMA systems. In Proceedings of 2nd IEEE International Conference on Universal Personal Communications (Vol. 2, pp. 970–974).

[6] Chen, C. C., Yao, K., & Biglieri, E. (2000). Optimal spread spectrum sequences constructed from Gold codes. In IEEE Global Telecommunications Conference (GLOBECOM).

[7] Fang, Y., Bi, G., Guan, Y. L., et al. (2015). A survey on protograph LDPC codes and their applications. IEEE Communications Surveys & Tutorials, 17(4), 1989–2016. https://doi.org/10.1109/COMST.2015.2436705

[8] Bae, J. H., Abotabl, A., Lin, H. P., et al. (2019). An overview of channel coding for 5G NR cellular communications. APSIPA Transactions on Signal and Information Processing, 8, e17. https://doi.org/10.1017/ATSIP.2019.10